

Coherent phase slips in coupled matter-wave circuits

A. Pérez-Obiol,^{1,*} J. Polo,^{2,*} and L. Amico^{2,3,4,5,†}

¹Barcelona Supercomputing Center, 08034 Barcelona, Spain[‡]

²Quantum Research Centre, Technology Innovation Institute, Abu Dhabi, UAE[§]

³INFN-Sezione di Catania, Via S. Sofia 64, 95127 Catania, Italy

⁴Centre for Quantum Technologies, National University of Singapore, 3 Science Drive 2, Singapore 117543, Singapore

⁵LANEF ‘Chaire d’excellence’, Université Grenoble-Alpes & CNRS, F-38000 Grenoble, France

(Dated: December 16, 2021)

Quantum Phase slips are dual process of particle tunneling in coherent networks. Besides to be of central interest for condensed matter physics, quantum phase slips are resources that are sought to be manipulated in quantum circuits. Here, we devise a specific matter-wave circuit enlightening quantum phase slips. Specifically, we investigate the quantum many body dynamics of two side-by-side ring-shaped neutral bosonic systems coupled through a weak link. By imparting a suitable magnetic flux, persistent currents flow in each ring with given winding numbers. We demonstrate that coherent phase slips occur as winding number transfer among the two rings, with the populations in each ring remaining nearly constant. Such a phenomenon occurs as a result of a specific entanglement of circulating states, that, as such cannot be captured by a mean field treatment of the system. Our work can be relevant for the observation of quantum phase slips in cold atoms experiments and their manipulation in matter-wave circuits. To make contact with the field, we show that the phenomenon has clear signatures in the momentum distribution of the system providing the time of flight image of the condensate.

Introduction Phase slips are jumps of the phase of the wave function. In coherent systems as superconducting and cold atoms networks, they occur because of the suppression of the amplitude of the superconducting/superfluid order parameter making the phase unrestricted and able to jump by a discrete amount (in multiples of 2π) [1, 2]. When such suppression is caused by thermal fluctuations, a thermal phase slip occurs. Quantum Phase Slips (QPS) instead, are induced by quantum fluctuations. A way to engineer QPS in mesoscopic physics is through Josephson junctions, in which such events correspond to tunneling of the phase of the order parameter [1, 3]. Intriguingly, relying on a phase-charge duality, it was argued that such tunneling events occur in proximity of the Coulomb blocked regime [4, 5].

In cold atoms settings, QPS have been investigated in different settings with enhanced control and flexibility of the physical conditions [6–10]. Atomtronic circuits, in particular, define coherent networks to study mesoscopic effects and quantum transport of ultracold atoms [11–15]. In the interesting configuration of bosonic condensates in a toroidal geometry, thermal and QPS have been suggested as the main responsible for the dynamics of the atoms’ persistent flow through the nucleation of vortex states and associated phonon emission, or through the formation of dark solitons activated thermally or by the stirring protocol [16–23].

Although over the past three decades several phenomena in superconducting networks have been related to

QPS’ formation [24–31], a convincing experimental evidence of their occurrence in solid state physics has been obtained only recently [32]. In cold atoms instead, QPS, as a coherent transfer of vortices or flux, have not been observed yet.

Besides their interest in fundamental physics, QPS can be a *resource* for quantum technology. Josephson junctions based quantum devices harnessing QPS have been carried out [31, 33, 34]. For atomtronic ring circuits interrupted by weak links, defining the atomic counterparts of SQUID devices, QPS localized at the weak link play a crucial role for creating the superposition of the current states that is expected to be especially important for quantum sensing [21, 35–39].

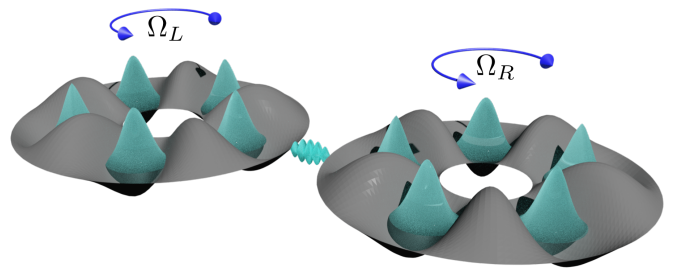


FIG. 1. Schematic diagram of an optical lattice consisting of two sided rings of five sites each. We represent the small link between rings, t_l , with a small interfering pattern connecting the rings. Both rings have an effective artificial gauge field denoted by Ω_L and Ω_R .

* Both authors contributed equally to this work

† On leave from Dipartimento di Fisica e Astronomia ‘Ettore Majorana’, Università di Catania, Italy

‡ axel.perezobiol@bsc.es

§ juan.polo@tii.ae

Relying on the considerable know-how achieved in magneto-optic circuit design and atom manipulation techniques, integrated atomtronic circuits define an interesting direction of the field [12, 13]. In this context, simple circuits of coupled rings and wave guides have

been considered [40–47]. Coupled ring condensates, in particular, are prototype systems for the definition of coherent cold atom networks in which matter wave flows are manipulated as a resource. Even though several attempts have been done in this direction, the analysis carried out so far show that independent winding numbers can co-exist in the two rings separately [46, 47]. The transfer of winding numbers, though, has not been achieved.

Here, we solve the above bottleneck and demonstrate a coherent QPS in two coupled rings arranged side-by-side as in Fig. 1. In the two rings, matter-wave currents with different winding numbers are assumed to be imparted through effective magnetic flux [48]. We will argue that to observe such effect it is important that the system works in the full-fledged quantum regime. Indeed, the QPS we observe results from an oscillation of entangled states of angular momentum states of the two rings.

The model. We consider a system of bosonic atoms trapped in two coupled coplanar rings lattice, each of N_s sites, and subjected to an effective magnetic flux Ω_α , $\alpha = L, R$. See Fig. 1 for a schematic picture of the system. The system's Hamiltonian reads

$$H = H_L + H_R + H_I(\tau),$$

$$H_\alpha = \sum_{i=0}^{N_s-1} \left[U(\hat{n}_{\alpha,i}^2 - \hat{n}_{\alpha,i}) - t \left(e^{-i\frac{2\pi\Omega_\alpha}{N_s}} \hat{a}_{\alpha,i}^\dagger \hat{a}_{\alpha,i+1} + h.c. \right) \right],$$

$$H_I(\tau) = -t_l(\tau) \left(\hat{a}_{L,0}^\dagger \hat{a}_{R,0} + \hat{a}_{R,0}^\dagger \hat{a}_{L,0} \right). \quad (1)$$

$\hat{a}_{\alpha,i}$ and $\hat{a}_{\alpha,i}^\dagger$ annihilate and create, respectively, a boson in the site i of the ring α , satisfying periodic conditions $\hat{a}_{\alpha,N_s} = \hat{a}_{\alpha,0}$, $\hat{a}_{\alpha,N_s}^\dagger = \hat{a}_{\alpha,0}^\dagger$, and the bosonic number operator is $\hat{n}_{\alpha,i} = \hat{a}_{\alpha,i}^\dagger \hat{a}_{\alpha,i}$. The parameters t and $U \geq 0$ are the intra-ring hopping amplitude and repulsive interaction; t_l describes the tunneling among the two rings. We set $t = 1$.

The limits $U = 0$ and $U \rightarrow \infty$ can be treated analytically for $t_l = 0$. The former reduces to the one particle problem, while the latter maps to tight-binding hard-core bosons[49]. We focus on the regime with weak inter-ring coupling $t_l < t$, allowing us to work out both the numerical simulations obtained by exact diagonalization and perturbative analysis in t_l/t .

For uncoupled symmetric rings, $t_l = \Omega_L = \Omega_R = 0$, the energy spectrum is invariant under the exchange of left and right states, or under the inversion of angular momentum directions in each separate ring, resulting in specific degeneracies in the spectrum of (1).

For $\Omega_L = \Omega_R > 0$, the rotational symmetry is broken, and clockwise and counterclockwise current states split into separate energy levels. In this regime, the eigenstates are found either non-degenerate or two-fold degenerate. A finite t_l splits the remaining degenerate energy levels, and the new eigenvectors become a superposition of the uncoupled degenerate states. We shall see that such level splitting is important for the formation of specific entangled states enabling the QPS (see supplemental for an example of such energy splittings).

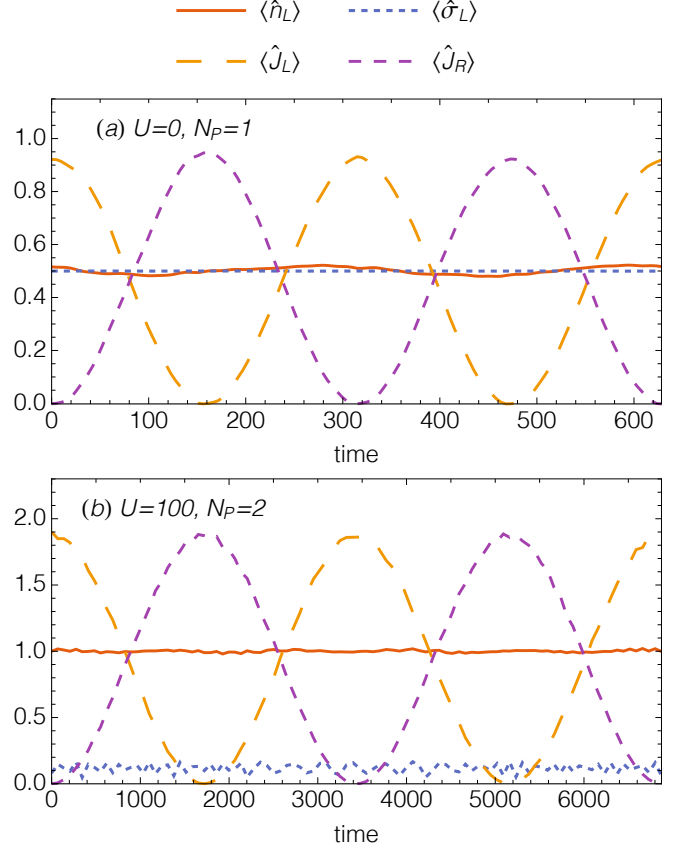


FIG. 2. Particle number's expectation, standard deviation, and current oscillations after quenching a system of two rings of five sites and initial fluxes $\Omega_L = 1$, $\Omega_R = 0$. The final velocities and interactions, particle number and t_l are (a) $\Omega_L = \Omega_R = 0.05$, $U = 0$, $N_p = 1$, $t_l = 0.05$ and (b) $\Omega_L = \Omega_R = 0.1$, $U = 100$, $N_p = 2$, $t_l = 0.1$ ($N_p > 2$ is considered in Fig. 4).

Quench Protocol. We first construct a state with the same density of particles in each ring, $\frac{N_p}{2}$, but with zero angular momentum on the right, $\langle J_R \rangle = 0$, and a non vanishing current on the left, $\langle J_L \rangle = J_{max}$. We denote such state as $|L_j; R_0\rangle \doteq |\frac{N_p}{2}, J_{max}; \frac{N_p}{2}, 0\rangle$, resulting to be an eigenstate of the system when $\Omega_L = j$, $\Omega_R = 0$, with j integer. Next, we perform the quench on the system to $\Omega_L = \Omega_R \gtrsim 0$. Then, the state $|L_j; R_0\rangle$ is a superposition of quasi-degenerate eigenvectors, each with the same particle number $\frac{N_p}{2}$ and total current J_{max} . After the quench, a time evolution occurs on the expectation value of the number of particles $\langle \hat{n}_\alpha \rangle$, its variance σ_α^2 , and the current $\langle J_\alpha \rangle$, defined as

$$\sigma_\alpha^2 = \langle \hat{n}_\alpha^2 \rangle - \langle \hat{n}_\alpha \rangle^2, \quad (2)$$

$$\langle J_\alpha \rangle = -i \sum_k \langle \hat{a}_{\alpha,k}^\dagger \hat{a}_{\alpha,k+1} - \hat{a}_{\alpha,k+1}^\dagger \hat{a}_{\alpha,k} \rangle, \quad (3)$$

with $\hat{n}_\alpha = \sum_i \hat{n}_{\alpha,i}$.

Results. Current oscillations between left and right rings are found for small and large interactions, $U \lesssim 0.01$

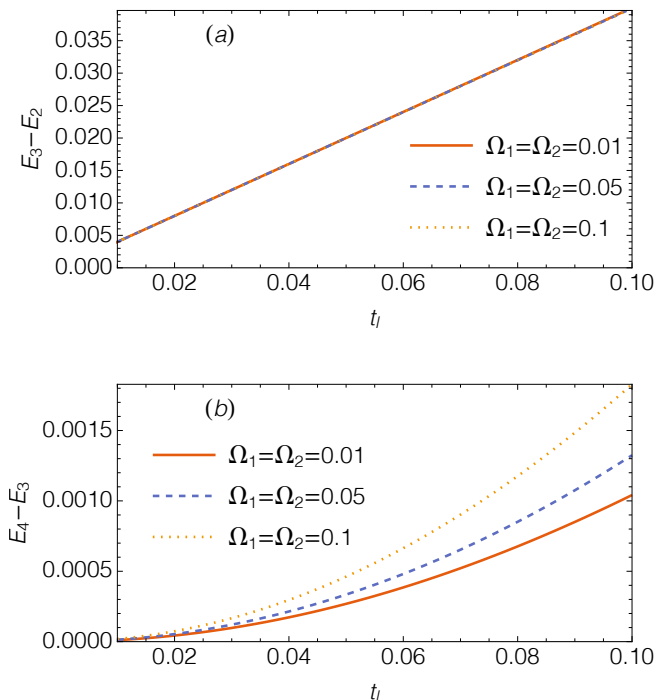


FIG. 3. Energy gap (such that $T = \frac{2\pi}{\Delta E}$, see supplemental material) as a function of the interring coupling t_l and $\Omega_L = \Omega_R = 0.01, 0.05, 0.1$ for: (a) one particle ($\Delta E = \frac{2t_l}{N_s}$), (b) two particles and $U = 100$ ($\Delta E \propto t_l^2$).

and $U \gtrsim 10$, when following the quench. See Fig. 2 for the cases $U = 0$ and $U = 100$. The currents in each ring oscillate completely out of phase, between a maximum value J_{max} and zero:

$$|L(\tau); R(\tau)\rangle = \cos(\omega\tau) |L_j; R_0\rangle + \sin(\omega\tau) |L_0; R_j\rangle, \quad (4)$$

with $\omega = \frac{\Delta E}{2\pi}$, ΔE being the energy gap between the involved states. Importantly, the expectation number $\langle \hat{n}_\alpha \rangle$ in each of the two rings results to be nearly constant at all times: *no net transfer of particles between rings occur and current oscillations happen due to the phase slipping through the weak link*. Note that the phase by itself does not carry any angular momentum or direction, and for the current to change an arbitrary small flux $\Omega_{L/R} = \Omega_\alpha$ is required to be applied in each ring.

The specific particle configuration n_α and σ_α^2 , and the maximum current J_{max} in $|L_j; R_0\rangle$ and $|L_0; R_j\rangle$ depend on U and N_p (see Table I and supplemental material). By using perturbation analysis, we find that ω depends linearly in t_l for $U = 0$, and quadratically for large U (except for odd N_p , see Fig. 3 and Table I). Important insights on the effect of the interaction can be obtained by studying the limit $U \rightarrow \infty$. Although the expected number of particles results to be barely affected by U , its variance σ_α does. For $U = 0$, $\sigma_\alpha^2 = \frac{N_p}{4}$. For large interactions, instead, any measurement of the occupation would always find half the particles in each ring, and

therefore $\sigma_\alpha^2 = 0$ is found (or $\frac{N_p \pm 1}{2}$ particles in each ring and $\sigma_\alpha^2 = \frac{1}{4}$ for N_p odd). We also remark that, because of the particle-hole symmetry holding for large interactions, QPS for holes occur similarly to the particles ones (see Fig. 4 and supplemental material). As for the maximum current, in the case $U = 0$, it results to scale linearly with the number of particles, $J_{max} = 2 N_p \sin\left(\frac{2\pi}{N_s}\right)$, while for large interactions we find $J_{max} = 4 \cos\left(\frac{\pi}{N_s}\right) \sin\left(\frac{\pi N_p}{N_s}\right)$. To transfer larger currents, one can simply start with an integer flux Ω_L in $1 < n < k_{max}$. Numerical tests for various ring sizes and initial currents corroborate that QPS are still found as N_p and angular momenta are increased (see Fig. 4 and supplemental material).

	$\langle \hat{n} \rangle$	σ^2	J_{max}	T
$U = 0$	$\frac{N_p}{2}$	$\frac{N_p}{4}$	$2 N_p \sin\left(\frac{2\pi}{N_s}\right)$	$\frac{\pi N_s}{t_l}$
$U \rightarrow \infty$	$\frac{N_p}{2}$	0	$4 \cos\left(\frac{\pi}{N_s}\right) \sin\left(\frac{\pi N_p}{N_s}\right)$	$\propto \frac{1}{t_l^2}$
	$\frac{1}{4}$			$\propto \frac{1}{t_l}$

TABLE I. Expected value of the occupation and variance in each ring, amplitude and period of current oscillations, in the case of no interactions and for $U \rightarrow \infty$.

By controlling t_l in time, and relying on our condition of weak ring-ring coupling, we note that different entangled states of angular momenta can be engineered by our scheme. The transfer of angular momentum can be obtained by manipulating t_l on $\tau = \frac{T}{2} \times (2n + 1)$. For $\tau = \frac{T}{4} \times (2n + 1)$, for example, the entangled state $|L_j; R_0\rangle + |L_0; R_j\rangle$ can be achieved.

Read-out of the QPS. Matter wave currents can be detected through time-of-flight (TOF) measurements [50, 51]. Such measurements in the far field are directly related to the momentum distribution at the moment in which the condensate is released from the ring trap. Therefore, the time evolution of the persistent current is reflected in the time evolution of the momentum distribution: $n(\mathbf{k}, t) = \sum_{i,j} e^{i\mathbf{k} \cdot (\mathbf{R}_i - \mathbf{R}_j)} C_{i,j}(t)$ with $C_{i,j}(t) = \langle \psi(t) | a_i^\dagger a_j | \psi(t) \rangle$ being the one-body correlation function between different sites and \mathbf{R}_j denoting the position of the lattice sites of the ring. In each ring, we find that $n(\mathbf{k}, t)$ evolves from a peak momentum distribution to the characteristic circular-shaped one as soon as the system acquires one unit of angular momentum. Such dynamics in the TOF provides the read-out of the transfer of coherent phase slips between zero and one unit of angular momentum. See Fig. 5.

Discussion and Conclusions. We have theoretically demonstrated QPS between two tunnel coupled rings of interacting bosons: We prepare two different phase-states of the two separated rings; after quenching the tunnel between the rings, we observe a coherent oscillation between the phase states with nearly vanishing population fluctuations (in each of the two rings). Once calibrated, the scheme can be used to produce, transfer, and entan-

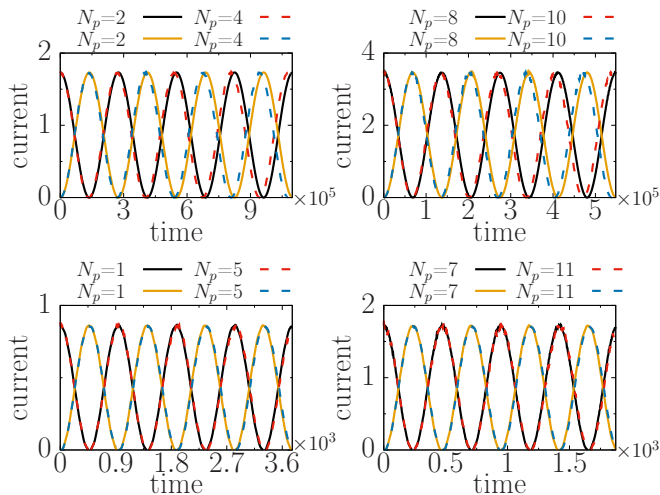


FIG. 4. Each plot compares QPS where (excess) particles N_e and holes $2N_s - N_e$ are exchanged in the strongly interacting regime, $U = 1000$, and in rings of $N_s = 3$ sites. Particle-hole symmetry is displayed for two different commensurate fillings, such that the total number of particles is $N_p = 2N_s \times N_b + N_e$, with $N_b = 0$ (left plots) and $N_b = 1$ (right plots), and $N_e = \{2, 4\}$ (top plots) and $N_e = \{1, 5\}$ (bottom plots). We quench from $\Omega_L = 1, \Omega_R = 0$, to $\Omega_L = 0.01, \Omega_R = 0.01$, and from $t_i = 10^{-5}$ to $t_f = 0.01$. Note that the period substantially changes for each commensurate filling $N_b = 0, 1$, despite having the same number of particles and holes. These changes appear because of the energy levels shift proportionally to N_b .

gle current states by tuning on and off the the weak link at specific times after the quenching protocol. We find that the phase slips faster from one ring to the other for stronger inter-ring couplings. Interactions reduce the maximum current in each ring, and make phase slips slower (see supplemental material for the interplay between interactions and period of oscillations). Indeed, such phenomenon occurs as a direct consequence of the entangled state created between the phase states of the two rings (macroscopic superposition of all particles rotating with different angular momenta in each ring). The coherent oscillations of the QPS are characterized by the simultaneous creation and destruction of current states in each ring (see Sec. A of supplemental material for specific examples). As such, QPS transfer is a genuine quantum effect that cannot be captured by standard mean-field analysis such as Gross-Pitaevskii based approach. In fact, the latter neglects entanglement and, to the best of our knowledge, cannot describe coherent transfer of matter-wave without transfer of population (which is an essential trait of our demonstration). We note that the coupling between the rings is perturbative and as such, the corresponding emergence of quasi-degenerate states involving a superposition of left and right current states hold for large particle numbers. The scope of our results can be further enlarged by resorting to a suitable

particle-hole symmetry. Therefore, our QPS are expected to occur also in systems with large particle numbers. We studied the momentum distribution that is the standard method to analyze neutral matter-wave currents in cold atoms experiments [50–55]

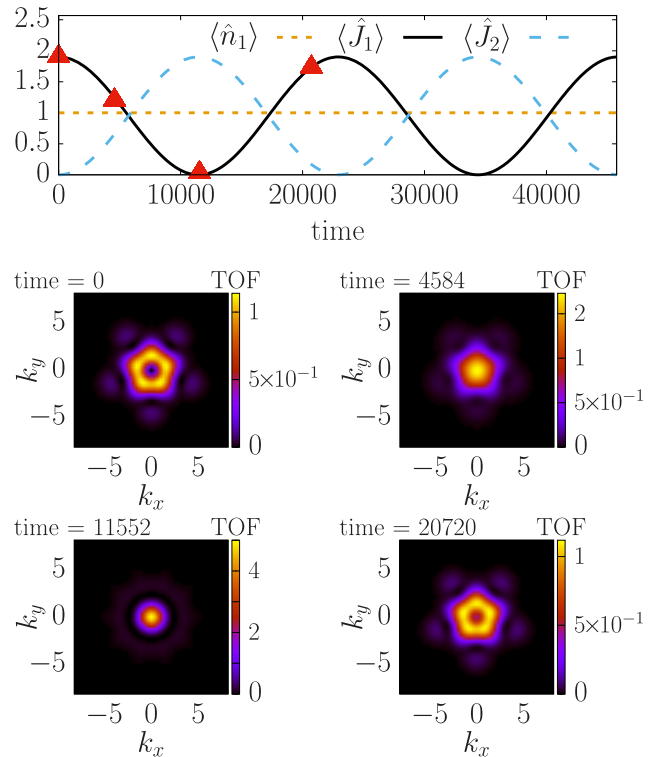


FIG. 5. Time-of-flight expansion of the left ring. Parameters are: $\Omega_L = 1, \Omega_R = 0$ to $\Omega_L = 0.01, \Omega_R = 0.01$, $t_i = 0$ to $t_f = 0.05$, $N_p = 2, N_s = 5$ in each ring, $U = 10$. Triangles indicate the times at which the TOF snapshots were taken.

Our work provides a specific platform to observe QPS in cold atoms that is a well known open problem in the field. At the same time, our work results are relevant to progress in the implementation of integrated atomtronic circuits [12, 13]. Specifically, our results effectively enable atomtronic circuit based on coupled atomic rings: In a sense analogue to the ‘Rapid Single Flux Quantum Logic’ conceived with SQUID’s [56], complex structures where the information is encoded in the phase slips inherent to the different rings could be implemented.

Acknowledgements. We thank Gianluigi Catelani and Wayne Jordan Chetcuti for discussion. A. P.-O. acknowledges financial support from Secretaria d’Universitats i Recerca del Departament d’Empresa i Coneixement de la Generalitat de Catalunya cofunded by the European Union Regional Development Fund within the ERDF Operational Program of Catalunya (project QuantumCat, ref. 001-P-001644).

-
- [1] K. Arutyunov, D. Golubev, and A. Zaikin, *Physics Reports* **464**, 1 (2008).
- [2] C. D’Errico, S. S. Abbate, and G. Modugno, *Philosophical Transactions of the Royal Society A: Mathematical, Physical and Engineering Sciences* **375**, 20160425 (2017).
- [3] G. Rastelli, I. M. Pop, and F. W. J. Hekking, *Phys. Rev. B* **87**, 174513 (2013).
- [4] J. Mooij and Y. V. Nazarov, *Nature Physics* **2**, 169 (2006).
- [5] A. M. Hriscu and Y. V. Nazarov, *Phys. Rev. B* **83**, 174511 (2011).
- [6] A. Polkovnikov, S. Sachdev, and S. M. Girvin, *Phys. Rev. A* **66**, 053607 (2002).
- [7] A. Polkovnikov, E. Altman, E. Demler, B. Halperin, and M. D. Lukin, *Phys. Rev. A* **71**, 063613 (2005).
- [8] S. Khlebnikov and L. P. Pryadko, *Physical review letters* **95**, 107007 (2005).
- [9] I. Danshita, *Phys. Rev. Lett.* **111**, 025303 (2013).
- [10] T. Roscilde, M. F. Faulkner, S. T. Bramwell, and P. C. W. Holdsworth, *New Journal of Physics* **18**, 075003 (2016).
- [11] L. Amico, G. Birkl, M. Boshier, and L.-C. Kwek, *New J. Phys.* **19**, 020201 (2017).
- [12] L. Amico and *et. al*, *AVS Quantum Science* **3**, 039201 (2021).
- [13] L. Amico, D. Anderson, M. Boshier, J.-P. Brantut, L.-C. Kwek, A. Minguzzi, and W. von Klitzing, *arXiv preprint arXiv:2107.08561* (2021).
- [14] J.-P. Brantut, J. Meineke, D. Stadler, S. Krinner, and T. Esslinger, *Science* **337**, 1069 (2012).
- [15] A. Burchianti, F. Scazza, A. Amico, G. Valtolina, J. A. Seman, C. Fort, M. Zaccanti, M. Inguscio, and G. Roati, *Phys. Rev. Lett.* **120**, 025302 (2018).
- [16] K. C. Wright, R. Blakestad, C. J. Lobb, W. D. Phillips, and G. K. Campbell, *Physical review letters* **110**, 025302 (2013).
- [17] A. Ramanathan, K. Wright, S. R. Muniz, M. Zelan, W. Hill III, C. Lobb, K. Helmerson, W. Phillips, and G. Campbell, *Physical review letters* **106**, 130401 (2011).
- [18] S. Eckel, J. G. Lee, F. Jendrzejewski, N. Murray, C. W. Clark, C. J. Lobb, W. D. Phillips, M. Edwards, and G. K. Campbell, *Nature* **506**, 200 (2014).
- [19] A. Yakimenko, Y. Bidasnyuk, M. Weyrauch, Y. Kuriatnikov, and S. Vilchinskii, *Physical Review A* **91**, 033607 (2015).
- [20] J. Polo, V. Ahufinger, F. W. J. Hekking, and A. Minguzzi, *Phys. Rev. Lett.* **121**, 090404 (2018).
- [21] J. Polo, R. Dubessy, P. Pedri, H. Perrin, and A. Minguzzi, *Phys. Rev. Lett.* **123**, 195301 (2019).
- [22] A. Pérez-Obiol and T. Cheon, *Phys. Rev. E* **101**, 022212 (2020).
- [23] A. Pérez-Obiol, J. Polo, and T. Cheon, *Phys. Rev. A* **102**, 063302 (2020).
- [24] C. N. Lau, N. Markovic, M. Bockrath, A. Bezryadin, and M. Tinkham, *Phys. Rev. Lett.* **87**, 217003 (2001).
- [25] A. Bezryadin, C. Lau, and M. Tinkham, *Nature* **404**, 971 (2000).
- [26] A. T. Bollinger, R. C. Dinsmore, A. Rogachev, and A. Bezryadin, *Phys. Rev. Lett.* **101**, 227003 (2008).
- [27] F. Altomare, A. M. Chang, M. R. Melloch, Y. Hong, and C. W. Tu, *Phys. Rev. Lett.* **97**, 017001 (2006).
- [28] N. A. Masluk, I. M. Pop, A. Kamal, Z. K. Mineev, and M. H. Devoret, *Phys. Rev. Lett.* **109**, 137002 (2012).
- [29] V. E. Manucharyan, J. Koch, L. I. Glazman, and M. H. Devoret, *Science* **326**, 113 (2009).
- [30] T. Weißl, B. Küng, E. Dumur, A. K. Feofanov, I. Matei, C. Naud, O. Buisson, F. W. J. Hekking, and W. Guichard, *Phys. Rev. B* **92**, 104508 (2015).
- [31] I. M. Pop, I. Protopopov, F. Lecocq, Z. Peng, B. Panetier, O. Buisson, and W. Guichard, *Nature Physics* **6**, 589 (2010).
- [32] O. Astafiev, L. Ioffe, S. Kafanov, Y. A. Pashkin, K. Y. Arutyunov, D. Shahar, O. Cohen, and J. S. Tsai, *Nature* **484**, 355 (2012).
- [33] J. E. Mooij and C. J. P. M. Harmans, *New Journal of Physics* **7**, 219 (2005).
- [34] A. Belkin, M. Belkin, V. Vakaryuk, S. Khlebnikov, and A. Bezryadin, *Phys. Rev. X* **5**, 021023 (2015).
- [35] M. Cominotti, D. Rossini, M. Rizzi, F. Hekking, and A. Minguzzi, *Phys. Rev. Lett.* **113**, 025301 (2014).
- [36] D. Aghamalyan, N. T. Nguyen, F. Auksztol, K. S. Gan, M. M. Valado, P. C. Condylis, L.-C. Kwek, R. Dumke, and L. Amico, *New J. Phys.* **18**, 075013 (2016).
- [37] L. Amico, D. Aghamalyan, F. Auksztol, H. Crepaz, R. Dumke, and L. C. Kwek, *Scientific Reports* **4** (2015), 10.1038/srep04298.
- [38] C. Ryu, P. W. Blackburn, A. A. Blinova, and M. G. Boshier, *Phys. Rev. Lett.* **111**, 205301 (2013).
- [39] J. Polo, P. Naldesi, A. Minguzzi, and L. Amico, *Quantum Science and Technology* **7**, 015015 (2021).
- [40] L. Amico, D. Aghamalyan, F. Auksztol, H. Crepaz, R. Dumke, and L. C. Kwek, *Scientific Reports* **4**, 4298 (2014).
- [41] S. Safaei, L.-C. Kwek, R. Dumke, and L. Amico, *Phys. Rev. A* **100**, 013621 (2019).
- [42] A. E. Mañas, A. Richaud, B. Juliá-Díaz, and M. Guilleumas, *Journal of Physics B: Atomic, Molecular and Optical Physics* (2021).
- [43] A. Richaud and V. Penna, *Phys. Rev. A* **96**, 013620 (2017).
- [44] D. Aghamalyan, L. Amico, and L. C. Kwek, *Physical Review A* **88**, 063627 (2013).
- [45] J. Polo, J. Mompert, and V. Ahufinger, *Phys. Rev. A* **93**, 033613 (2016).
- [46] G. Pelegrí, A. M. Marques, V. Ahufinger, J. Mompert, and R. G. Dias, *Phys. Rev. B* **100**, 205109 (2019).
- [47] T. Bland, Q. Marolleau, P. Comaron, B. Malomed, and N. Proukakis, *Journal of Physics B: Atomic, Molecular and Optical Physics* **53**, 115301 (2020).
- [48] J. Dalibard, F. Gerbier, G. Juzeliūnas, and P. Öhberg, *Rev. Mod. Phys.* **83**, 1523 (2011).
- [49] Y. Wu and X. Yang, *J. Opt. Soc. Am. B* **23**, 1888 (2006).
- [50] S. Moulder, S. Beattie, R. P. Smith, N. Tammuz, and Z. Hadzibabic, *Phys. Rev. A* **86**, 013629 (2012).
- [51] L. Amico, A. Osterloh, and F. Cataliotti, *Phys. Rev. Lett.* **95**, 063201 (2005).
- [52] M. Greiner, O. Mandel, T. Esslinger, T. W. Hänsch, and I. Bloch, *Nature* **415**, 39 (2002).
- [53] F. Gerbier, A. Widera, S. Fölling, O. Mandel, T. Gericke, and I. Bloch, *Phys. Rev. A* **72**, 053606 (2005).
- [54] Y. Kato, Q. Zhou, N. Kawashima, and N. Trivedi, *Nature Physics* **4**, 617 (2008).

- [55] A. Hoffmann and A. Pelster, [Phys. Rev. A **79**, 053623 \(2009\)](#).
- [56] K. K. Likharev and V. K. Semenov, IEEE Transactions on Applied Superconductivity **1**, 3 (1991).

Appendix A: Single particle analytical results in Fourier space

For one particle and $\Omega_L = 1$, the initial state is $|\psi_+\rangle = \frac{1}{\sqrt{2}}(b_{L,1}^\dagger + b_{R,0}^\dagger)|0\rangle$, where $b_{\alpha,l}^\dagger = \frac{1}{\sqrt{N_s}} \sum_j e^{i\frac{2\pi(jl)}{N_s}} a_{\alpha,j}^\dagger$ creates a particle with momentum l in the ring α . It has an average particle number per ring $n_\alpha = \frac{1}{2}$ and variance $\sigma_\alpha^2 = \frac{1}{4}$. In this case, H_{BH} in momentum space consists of a diagonal term, where the eigenvectors are vortex states, $b_{\alpha,i}^\dagger|0\rangle$, and a perturbative one, that transfers momentum modes between left and right rings,

$$H_{BH} = -2 \sum_{\alpha=L,R} \sum_{i=0}^{N_s-1} \cos(2\pi(i - \Omega_\alpha)/N_s) \hat{b}_{\alpha,i}^\dagger \hat{b}_{\alpha,i} - \frac{t_l}{N_s} \sum_{i,j=0}^{N_s-1} \left(\hat{b}_{L,i}^\dagger \hat{b}_{R,j} + h.c. \right). \quad (\text{A1})$$

The energy gap is $\Delta E = \langle \psi_- | H_p | \psi_- \rangle - \langle \psi_+ | H_p | \psi_+ \rangle = \frac{2t_l}{N_s} + \mathcal{O}(t_l^2)$, where H_p is the second term of Eq. (A1) and $|\psi_-\rangle = \frac{1}{\sqrt{2}}(b_{L,1}^\dagger - b_{R,0}^\dagger)|0\rangle$. If $U = 0$, each particle behaves independently, and current oscillations are due to the simultaneous but opposite transfer of the ground and first excited momentum modes. The particle distribution is binomial, with $n_\alpha = \frac{N_p}{2}$ and variance $\sigma_\alpha^2 = \frac{N_p}{4}$. The initial (and maximum) current scales with the number of particles, and evaluates to $J_{max} = 2 N_p \sin\left(\frac{2\pi}{N_s}\right)$.

Appendix B: Two-state level simplification

All the current oscillations found can be understood in terms of dynamics within a system of two quasi-degenerate states. For a given set of fluxes, $\Omega_L = \Omega_R = \Omega \gtrsim 0$, and a weak enough interring coupling, $t_l \gtrsim 0$, pairs of quasi-degenerate states can effectively be treated as uncoupled from the rest of eigenstates. Here we show this explicitly with two specific examples, one for $U = 0$, which reduces to the case of one particle, and another for large interactions, $U \rightarrow \infty$.

In the case of one particle, terms coupling different momentum modes in Eq. (A1) enter at order $\mathcal{O}(t_l)$ when diagonalizing, assuming single ring energy levels $E_i = -2t \cos(2\pi(i - \Omega)/N_s)$ are separate enough. Neglecting those terms, H_{BH} can be written in terms of two-mode independent Hamiltonians,

$$H_{BH}^{(i)} = E_i \left(\hat{b}_{L,i}^\dagger \hat{b}_{L,i} + \hat{b}_{R,i}^\dagger \hat{b}_{R,i} \right) - \frac{t_l}{N_s} \left(\hat{b}_{L,i}^\dagger \hat{b}_{R,i} + h.c. \right). \quad (\text{B1})$$

Within this picture, the ground and first excited states are $|\phi_0^\pm\rangle = \frac{1}{\sqrt{2}}|0,1\rangle \pm \frac{1}{\sqrt{2}}|1,0\rangle$, where $|N_L, N_R\rangle$ define states with N_L static particles in the left ring and N_R in the right one. Equivalently, the next excited states

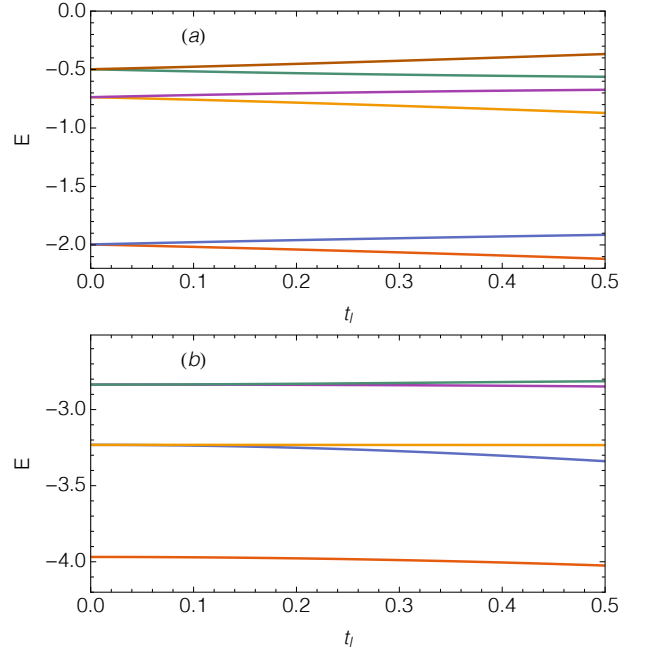


FIG. 6. Energy levels as a function of the interring coupling t_l for (a) $U = 0$, $\Omega_1 = \Omega_2 = 0.05$, $N_p = 1$ and (b) $U = 100$, $\Omega_1 = \Omega_2 = 0.1$, $N_p = 2$. In (a), the corresponding eigenstates are, from bottom to top, $|\phi_0^+\rangle$, $|\phi_0^-\rangle$, $|\phi_1^+\rangle$, $|\phi_1^-\rangle$, $|\phi_{-1}^+\rangle$, and $|\phi_{-1}^-\rangle$, as described in the main text. The first and second energy splittings are separated by $E_1 - E_0 = -2 \cos(2\pi(1 - \Omega)/N_s) + 2 \cos(2\pi(\Omega)/N_s)$, while the gap between the second and third is $\Delta\epsilon_\Omega = \frac{8\pi}{N_s} \sin\left(\frac{2\pi j}{N_s}\right) \Omega + \mathcal{O}(\Omega^3)$. In (b), the energy levels correspond to eigenstates $|\chi_0\rangle$, $|\chi_0^+\rangle$, $|\chi_0^-\rangle$, $|\chi_1^+\rangle$, and $|\chi_1^-\rangle$.

are $|\phi_1^\pm\rangle = \frac{1}{\sqrt{2}}|0,1^+\rangle \pm \frac{1}{\sqrt{2}}|1^+,0\rangle$. Here the subindex 1 in ϕ and superindex + in 1 indicate one unit of angular momentum in the direction of Ω . These pair of eigenstates are energetically separate from $|\phi_0^\pm\rangle$, and from the next excited states, $|\phi_{-1}^\pm\rangle = \frac{1}{\sqrt{2}}|0,1^-\rangle \pm \frac{1}{\sqrt{2}}|1^-,0\rangle$, in which the rotation is opposite to the fluxes Ω (see Fig. 6 (a)). These energy gaps are much larger than the energy separating $|\phi_1^-\rangle$ and $|\phi_1^+\rangle$ states in each pair, which is $\Delta E = \frac{2t_l}{N_s}$ in all cases. The evolution of the initial state from our protocol, $|\psi_+\rangle = \frac{1}{\sqrt{2}}|1^+,0\rangle + \frac{1}{\sqrt{2}}|0,1\rangle$, consists of two independent evolutions with the same frequency $\omega = \frac{\Delta E}{2\pi}$, one for $|1^+,0\rangle$, and another for $|0,1\rangle$,

$$|\psi(\tau)\rangle = \frac{e^{-iE_1\tau}}{\sqrt{2}} [\cos(\omega\tau)|1^+,0\rangle + i\sin(\omega\tau)|0,1^+\rangle] + \frac{e^{-iE_0\tau}}{\sqrt{2}} [\cos(\omega\tau)|0,1\rangle + i\sin(\omega\tau)|1,0\rangle] \doteq \cos(\omega\tau)|L_1;R_0\rangle + \sin(\omega\tau)|L_0;R_1\rangle. \quad (\text{B2})$$

For large interactions and even N_p , eigenstates have the same number of particles $N = \frac{N_p}{2}$ in each ring. The ground state is $|\chi_0\rangle = |N,N\rangle$, energetically separate from the first excited states, among which

are $|\chi_1^\pm\rangle = \frac{1}{\sqrt{2}}|N, N^+\rangle \pm \frac{1}{\sqrt{2}}|N^+, N\rangle$, and $|\chi_{-1}^\pm\rangle = \frac{1}{\sqrt{2}}|N, N^-\rangle \pm \frac{1}{\sqrt{2}}|N^-, N\rangle$. In this case the energy gap ΔE separating $|\chi_i^+\rangle$ and $|\chi_i^-\rangle$ states is much smaller and proportional to t_l^2 , see Fig. 6 for the case with $N = 1$ in each ring. Given an initial state $|\psi(t=0)\rangle = |N^+, N\rangle$, it evolves with a relatively low frequency $\omega = \frac{\Delta E}{2\pi}$,

$$|\psi(\tau)\rangle = e^{-i E_1 \tau} [\cos(\omega \tau) |N^+, N\rangle + i \sin(\omega \tau) |N, N^+\rangle] \\ \doteq \cos(\omega \tau) |L_1; R_0\rangle + \sin(\omega \tau) |L_0; R_1\rangle. \quad (\text{B3})$$

Appendix C: Spectrum for large interactions

The spectrum for $U = 0$ does not depend on the number of particles, N_p , and the relevant energy gap and evolution after the quench can be computed analytically with first order perturbation theory. In contrast, for large interactions, the energy gaps do depend on N_p , and scale as t_l^2 , instead of t_l , which implies that second-order perturbation theory is needed. In this section we analyze how the spectrum for large interactions depends on Ω_α , t_l , U , and N_p .

The energy spectrum for two particles and $\Omega_R \gtrsim 0$ as a function of Ω_L is plotted in Fig. 7. At $\Omega_L = \Omega_R \gtrsim 0$, states are symmetric with respect to the exchange of left and right rings. They correspond to, from bottom to top and in the same notation as in Appendix B,

$$|\chi_0\rangle = |1, 1\rangle, \\ |\chi_0^+\rangle = \frac{|0, 2\rangle + |2, 0\rangle}{\sqrt{2}}, \quad |\chi_0^-\rangle = \frac{|0, 2\rangle - |2, 0\rangle}{\sqrt{2}}, \\ |\chi_1^+\rangle = \frac{|1, 1^+\rangle + |1^+, 1\rangle}{\sqrt{2}}, \quad |\chi_1^-\rangle = \frac{|1, 1^+\rangle - |1^+, 1\rangle}{\sqrt{2}}, \\ |\chi_{-1}^+\rangle = \frac{|1, 1^-\rangle + |1^-, 1\rangle}{\sqrt{2}}, \quad |\chi_{-1}^-\rangle = \frac{|1, 1^-\rangle - |1^-, 1\rangle}{\sqrt{2}}. \quad (\text{C1})$$

As Ω_L increases, this symmetry is broken, and eigenvectors turn to, approximately, $|1, 1\rangle$, $|0, 2\rangle$, $|2, 0\rangle$, $|1^+, 1\rangle$, $|1, 1^+\rangle$, $|1, 1^-\rangle$, $|1^-, 1\rangle$. The energies increase quadratically with Ω_L , except for the state in which the left ring is empty, $|0, 2\rangle$, in which the energy remains constant. At $\Omega_L \lesssim 1$, we have the same states except for a general shift in one unit of angular momentum in the right ring. As Ω_L decreases from $\Omega_L = 1$, states with particles on the left also increase their energy quadratically. Due to the small but finite t_l , the energy levels have avoided crossings (some are too small to see in the figure). In terms of the relation between the ground state at $\Omega_L = 1$, $|1^+, 1\rangle$, the initial state in our protocol, with the states at $\Omega_L \gtrsim 0$, these avoided crossings imply $|1^+, 1\rangle = \frac{1}{\sqrt{2}}|\chi_1^+\rangle + \frac{1}{\sqrt{2}}|\chi_1^-\rangle$.

The corresponding energy gap, $\Delta E = E_4 - E_3$, is plotted as a function of U and t_l in Fig. 8. At $U = 0$, ΔE is relatively large and shows no dependence on t_l . In this case, the energy gap between the third and fourth excited

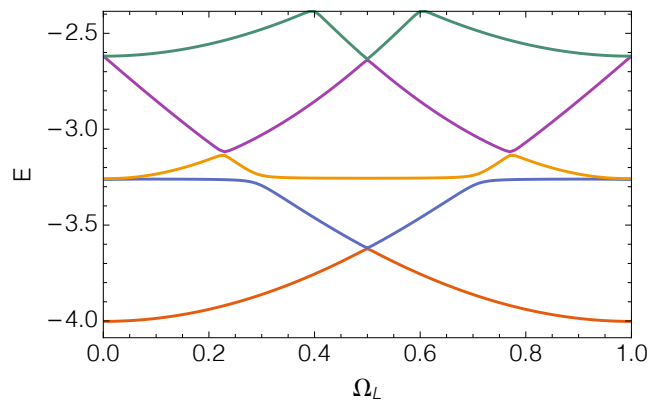


FIG. 7. Spectrum of energies depending on Ω_L (left) for $U = 100$, $N_p = 2$, $t_l = 0.1$, and $\Omega_R = 0$. A quench can be made such that the ground state at $\Omega_L = 1$ is a superposition of the third and fourth excited states at $\Omega_L = 0$.

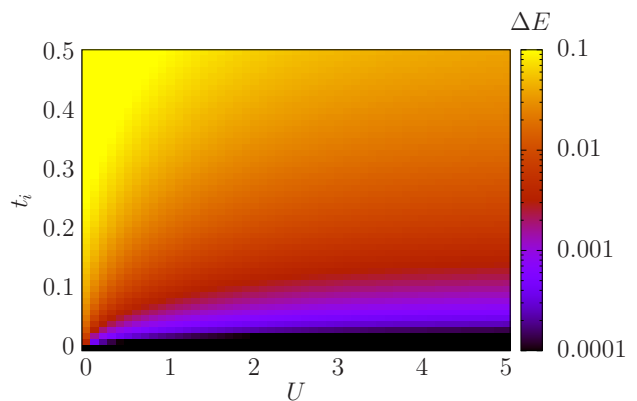


FIG. 8. Energy gap of the two occupied states as a function of the link strength t_l and interactions U after a quench starting from $\Omega_L = 1$, $\Omega_R = 0$ to $\Omega_L = \Omega_R = \Omega_j = 0.1$ for $N_p = 2$ particles and $N_s = 5$. All curves collapse for large enough interactions and the gap behaves equally as a function of t_l .

states corresponds to ΔE_Ω (See Fig. 6). As interactions U increase, the energy gap ΔE closes and its dependence on t_l converges to a fixed gradient.

As for the dependence of ΔE on N_p , it exhibits two main features. First, the energy gaps for N_p even are much smaller than for N_p odd, the former being proportional to t_l^2 and the latter to t_l . Second, the energy gaps are the same under the exchange of particles and holes. For large interactions, the BH model maps to a spinless FH model, in which the spectrum is invariant, except for a general shift, under the exchange $N_p \leftrightarrow 2N_s - N_p$. This implies that, in the case of rings with five sites, the spectra and energy gaps are the same for the pairs of particle numbers $N_p = 1, 9$; $2, 8$; $3, 7$; and $4, 6$. Apart from the symmetry under the exchange $N_p \leftrightarrow 2N_s - N_p$, we find the energy gap is largest at smallest or largest occupations, and decreases down to a minimum at half filling.

Particle-hole symmetry still holds when $N_p > 2N_s$,

as shown in Fig. 4 in the main text. If there are more particles than sites, such that there is a number $2N_s \times N_b$ of particles evenly distributed in the background, and N_e excess particles, $N_p = 2N_s \times N_b + N_e$, the energy gap as a function of N_e has the same qualitative behavior. Therefore, ring systems with more particles than sites have very similar behavior in terms of phase slips. If $N_e = 0$, as in the case of full filling, the ground state has N_b particles per site, and is energetically very separate from the first excited state (the gap being proportional to U , which we assume large). In this case, our protocol does not allow for phase slips.